专业生词部分的注释—棕色填充

Bioresource Technology 261 (2018) 36–43

Contents lists available at ScienceDirect

Bioresource Technology

journal homepage: www.elsevier.com/locate/biortech

# Enhancing microalgae biofilm formation and growth by fabricating microgrooves onto the substrate surface

Yun Huang[a,b], Yaping Zheng[a,b], Jun Li[a,b], Qiang Liao[a,b,*], Qian Fu[a,b], Ao Xia[a,b], Jingwei Fu[a,b], Yahui Sun[a,b]

[a] Key Laboratory of Low-grade Energy Utilization Technologies and Systems, Chongqing University, Ministry of Education, Chongqing 400044, China
[b] Institute of Engineering Thermophysics, Chongqing University, Chongqing 400044, China

## GRAPHICAL ABSTRACT

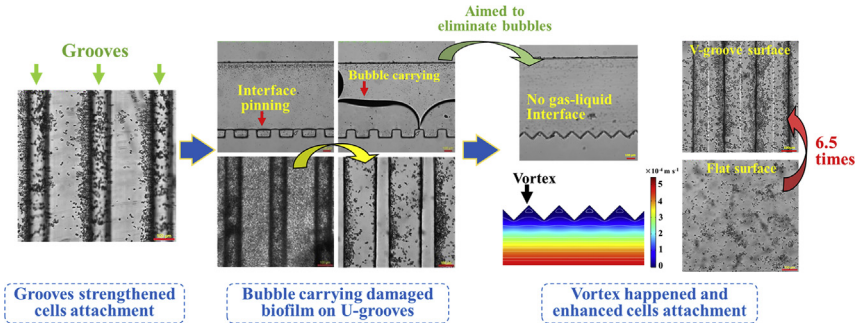


## ARTICLE INFO

*Keywords:*
Microalgae biofilm
Microgrooves substrate
Attachment strength
Hydrodynamics

## ABSTRACT

Attachment of cells to substrate surface is the premise for biofilm formation. To shelter microalgae cells from fluid shear stress and offer larger areas for microalgae attachment, the inerratic microgrooves, which can act as anchor points that offer larger areas for microalgae attachment and induce vortex to protect cells from hydraulic shear stress, were designed and fabricated into substrate surface. The results indicated that the shear stress on the surface with V-grooves was weaker than that on the surface with U-grooves, and 45° V-grooves with the width of 200 μm were benefit for cells attachment. The initial attachment time was shortened to 50 min under the hydraulic shear stress of 0.02 Pa compared to that of 135 min on the surface without microgrooves. Subsequently, the biofilm biomass concentration on the surface with 45° V-grooves increased by 14.29% to 165.84 g $m^{-2}$ compared with that on flat substrates.

## 1. Introduction

Microalgae have significant potential for $CO_2$ capture and high value-added bioproducts production (Sun et al., 2018). However, the high costs of microalgae harvesting and dewatering, have been regarded as the key challenges for microalgae industry development (Liao et al., 2018). In recent decades, there is a great interest in a new microalgae cultivation mode, biofilm cultivation. For this mode, the dense microalgae communities attached and multiplied on the solid substrate surfaces, then formed the mature biofilm. Therefore, it could separate the aqua-medium and the high concentration of biomass, which made it easily to harvest and significantly reduced the cost of microalgae harvesting (Zheng et al., 2017).

Microalgae biofilm forms from the attachment of planktonic cells,

* Corresponding author at: Key Laboratory of Low-grade Energy Utilization Technologies and Systems, Chongqing University, Ministry of Education, Chongqing 400044, China.
*E-mail address:* lqzx@cqu.edu.cn (Q. Liao).

https://doi.org/10.1016/j.biortech.2018.03.139
Received 5 February 2018; Received in revised form 29 March 2018; Accepted 30 March 2018
Available online 05 April 2018
0960-8524/ 

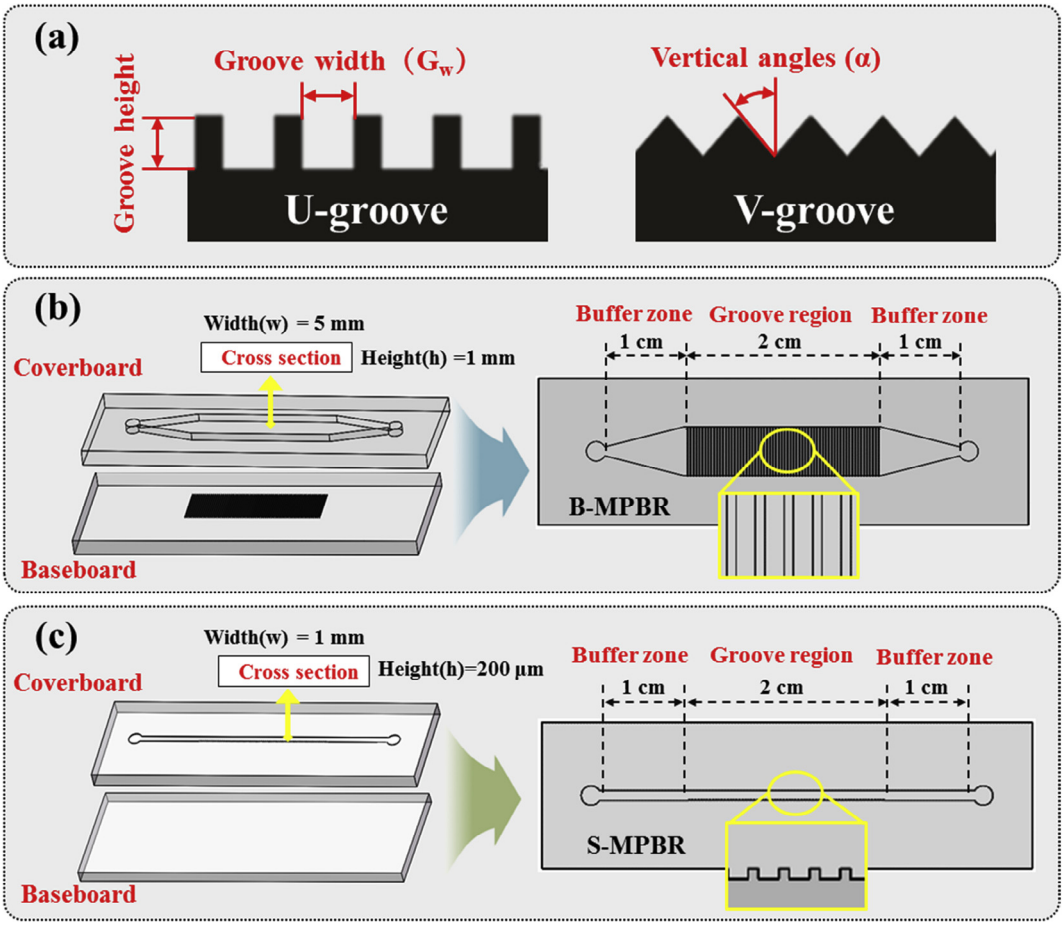


**Fig. 1.** Schematics of groove substrates and the microphotobioreactors with grooves at the bottom surface (B-MPBR) and on the side (S-MPBR).

which move around to the solid substrate surfaces. Nevertheless, microalgae cells without flagella can only passively move along with hydrodynamic flow instead of active movement. On the one hand, dynamic medium can optimize the nutrient conditions around the attached biofilm. On the other hand, hydrodynamic shear stress suppresses the development of a biofilm matrix. Thus, hydrodynamic conditions can have contradictory influences on biofilm development (Kim et al., 2012; Zhang et al., 2010). The patterns on the substrate can not only increase the special area and offer larger areas for cells attachment, but also act as anchor points sheltered cells from shear stresses (Schnurr and Allen, 2015). Thus, in order to reduce the negative effects of shear stress on biofilm, quite a few researchers patterned the substrate surfaces and investigated the effects of the topography on biofilm formation. The previous studies have investigated the bacteria biofilm attachment on substrate surfaces with different topography, such as irregular surfaces, etching surfaces with arrays of diamond-shaped and heart-shaped holes, latticed surfaces, grooved surfaces and so on (Crawford et al., 2012; Eun and Weibel, 2009; Hou et al., 2011). The results confirmed that preferential attachment of cells occurred on the appropriate patterned surfaces compared to flat surfaces. To date, the relevant researches for microalgae biofilm mainly focused on anti-biofouling field (Bing et al., 2016; Ngene et al., 2010). The surface topographies were designed and chosen to resist microalgae attachment and reduce the fouling of material surfaces. However, with the rise of microalgae biofilm cultivation, it urgently needs to find out the surface topographies that benefit for microalgae attachment and growth.

Shen et al. (2013) investigated microalgae biofilm growth on nine different materials. They found microalgae cells formed and grew better on the glass fiber-reinforced plastic. Unfortunately, they failed to clarify the natural and irregular surface topographies on these materials. Thus, the effects of substrate topography on biofilm form were not exploded. Then, Cao et al. (2009) used laser textured stainless steel surfaces with dimples sizes of 250–1000 μm in diameter to investigate effects of surfaces microstructures on microalgae attachment. The results suggested surfaces topography enhanced microalgae and cells could attach on some certain size dimples. However, the researches only analyzed the results via several photographs in general terms and didn't quantize the dimple sizes and the adhesion amount of microalgae cells. In order to further study the effects of surface topography on biofilm attachment and growth, Kardel (2016) adopted 3D-printing technology to form adjacent hemispheres of 500–2000 μm peak gaps. The results showed that biofilm on the patterned surfaces grew better than that on flat section. Especially, microalgae biomass productivity was significantly higher on the sections of 500 μm peak gaps than that on other sections. Furthermore, Sathananthan et al. (2013) tested 3 micro-structured substrates on microalgae biofilm growth, and obtained that surface patterns that were of the same size scale as the microalgae cells resulted in higher biomass productivity. However, there are still few explanations for the good growth performance of microalgae on the surfaces with micro-scale patterns. It is still unclear how the micro-scale patterns help microalgae cells resist hydrodynamics shear stress during microalgae biofilm formation. On the other hand, the studies almost didn't comprehensively consider the substrate effects on microalgae biofilm with both initial attachment and long-term growth period. Thus, the research conclusions were somewhat inconclusive and controversial (Gross et al., 2015).

Thereby, in this study, the different sizes (100–200 μm in height and 200–500 μm in depth) and shapes (U-grooves and V-grooves) of microgrooves were designed and fabricated by 3D-printing and microlithography technologies. The initial attachment process of microalgae

cells on microgrooves was experimentally studied in microphotobioreactors (MPBRs) by an optical microscope. In addition, the hydrodynamic shear stresses in the MPBRs were calculated via a CFD to further comprehend the effects of microgrooves on biofilm development processes. Finally, the effects of microgrooves substrate on microalgae biofilm were investigated at a long-term growth period in a cycling biofilm cultivation system.

## 2. Methods and materials

### 2.1. Microalgae strains and cultivation

The microalgae *Scenedesmus obliquus* (FACHB-417) used in this study was purchased from the Institute of Hydrobiology, Chinese Academy of Sciences (Wuhan, China). The cells were maintained in Blue-Green medium (BG11) (Gao et al., 2015). The media was sterilized at 121 °C for 20 min, then the pH was adjusted to 7.0 with 0.1 M HCl. The Erlenmeyer flasks were cultivated at 25 °C under a light intensity of 90 μmol $m^{-2} s^{-1}$.

### 2.2. Design and fabrication of experiment device

The substrate surfaces were fabricated with different grooves, which shaped as U-grooves and V-grooves (Fig. 1a). The heights of U-grooves were 100 μm and 200 μm, while the width changed from 200 μm to 500 μm. For the V-grooves, the grooves height was 100 μm and the vertical angles (α) were 20°, 30°, 45° and 60°. The schematics of the MPBRs were shown in Fig. 1b and c. The microphotobioreactors with grooves at the bottom surface (B-MPBR) were designed for the initial attachment study (Fig. 1b). The area of grooves section was 20 mm × 5 mm. To ensure the liquid flow uniform and stable, the buffers ($10^{-3}$ m) were appended beside both sides of the grooves section. The height of B-MPBR was $10^{-4}$ m. In order to observe liquid flow state, the microphotobioreactor with grooves on the side (S-MPBR) were designed as a 200 μm longitudinal section of B-MPBR along velocity direction (Fig. 1c).

In this study, MPBRs were fabricated via soft lithography as described in the previous study (Ahsan et al., 2014). The B-MPBR molds of the baseboard and cover board were manufactured by 3D printing respectively. The molds of S-MPBR were fabricated using SU-8 photoresist on a silicon. Then, the prepared polydimethylsiloxane (PDMS) was poured into the molds and cured at 85 °C for 10 min. After cooling, the PDMS replicas were lifted off from the molds and punched the medium inlet and outlet. Finally, the baseboard and cover board were bonded together as a MPBR.

### 2.3. Experimental setup and analytical methods

#### 2.3.1. Biofilm formation and biofilm attachment strength analysis

The visualization experiments were conducted in the MPBRs with an inverted microscope (IX81, Olympus) to investigate the biofilm formation and attachment strength. In order to clearly inspect the process of biofilm formation, the low concentration microalgae suspension (0.22 g $L^{-1}$) was inoculated into the B-MPBRs with different inlet flow rate (100–500 μl $min^{-1}$). During this process, the planktonic cells attached onto the substrate surfaces, so that the biofilm coverage areas increased over time. The initial attachment process finished until the substrate surfaces were fully covered, that is, the biofilm coverage areas reached to 100%. Meanwhile, the microalgae suspension were inoculated into the S-MPBRs with the inlet flow rate from 20 μl $min^{-1}$ to 100 μl $min^{-1}$ for fluid observation. Although the sizes of the two type MPBRs were different, the Reynolds numbers of the inoculated flow were the same, as shown in Table1. Re was calculated with Eq. (1):

$$\mathrm{Re} = \rho V_{in} d/\mu \quad (1)$$

where ρ ($10^{3}$ kg $m^{-3}$) and μ ($8.937 \times 10^{-4}$ Pa·s) were the dynamic viscosity coefficient and density of microalgae suspension, respectively. For the low concentration of microalgae suspension, the physical property parameters are basically the same with that of water (Chen et al., 2017). And the flow velocity at the inlet of the MPBR was denoted as $V_{in}$ (m $s^{-1}$) and expressed as Eq. (2). The hydraulic diameter, $d$ (m), was calculated with Eq. (3)

$$V_{in} = Q_{in}/wh \quad (2)$$

$$d = 2wh/w + h \quad (3)$$

In which, $Q_{in}$ (m $s^{-1}$) is the inlet flow rate, $w$ is the MPBR width ($10^{-3}$ m) and $h$ is the B-MPBR height ($2 \times 10^{-4}$ m).

Furthermore, the shear stress, τ (Pa), is calculated with Eq. (4), in which γ ($s^{-1}$) is the shear rate.

$$\tau = \mu \times \gamma \quad (4)$$

After The initial attachment of microalgae biofilm, the attachment strength was investigated. The sterile water was injected into the B-MPBRs with a high inlet flow rate (1 ml $min^{-1}$). The shear stress of top edge of the grooves sections was 0.02 Pa calculated by CFD. During this washing process, the floating and weakly bound cells were removed gradually, only strongly-attached cells remained. Thus, the percentage of remaining biofilm could be obtained to evaluate the biofilm attachment strength (Carl et al., 2012; Park et al., 2011).

The obtained biofilm microscope images were analyzed using Matlab software. These images were firstly converted into grayscale, and then the interference was removed using a background subtraction method (Zhao et al., 2015). Finally, the biofilm coverage areas were extracted and calculated based on a range of gray values.

**Table 1**
Reynolds numbers in two kinds of MPBRs with different inlet flow rate.

| Re | 0.62 | 1.24 | 1.86 | 2.48 | 3.11 |
|---|---|---|---|---|---|
| Inlet flow rate in B-MPBRs (μl $min^{-1}$) | 100 | 200 | 300 | 400 | 500 |
| Inlet flow rate in S-MPBRs (μl $min^{-1}$) | 20 | 40 | 60 | 80 | 100 |

#### 2.3.2. Biofilm growth analysis

The biofilm cultivation system as described in detail in the authors' previous study (Zheng et al., 2016) was used in this study for *S. obliquus* biofilm cultivation. The optimal microgrooves substrates selected in the former experiment were fixed at the bottom of photobioreactors (PBRs). 45 ml of microalgae suspension with a concentration of 0.33 g $L^{-1}$ was inoculated into each PBR. 5% $CO_2$ was aerated into the BG11 medium and sufficiently dissolved in a mixing Erlenmeyer flask. Then, the premixed medium was pumped into each PBR. The outflow medium was collected and pumped back into the mixing Erlenmeyer flask. In order to investigate the effects of inlet flow rate on biofilm formation, the Re of circulating medium were changed with 0.62, 1.86 and 3.11. During the biofilm growth, two parallel samples were sampled every 2 days for microalgae biomass concentration analysis. In order to measurement, the supernatant medium in the MPBR was firstly removed and then the microalgae biofilm on the substrate surfaces with grooves were washed into a 25 ml volumetric flask with sterile distilling water. The biomass concentration of biofilm was measured based on the biomass dry weight collected in the flask (Shayan et al., 2016).

#### 2.3.3. Fluid dynamics analysis

In this study, a CFD software was used to simulate the hydrodynamics of the liquid in the MPBRs. The average flow velocity and shear stress on the grooves sections were extracted from the simulation. According to the geometry of B-MPBRs and to reduce computational cost, only 2D domain was modeled: a longitudinal section of B-MPBR along velocity direction. The computational domain was discretized using the unstructured meshes and many finer grids were utilized near the grooves regions. According to the inlet flow rate, a laminar model

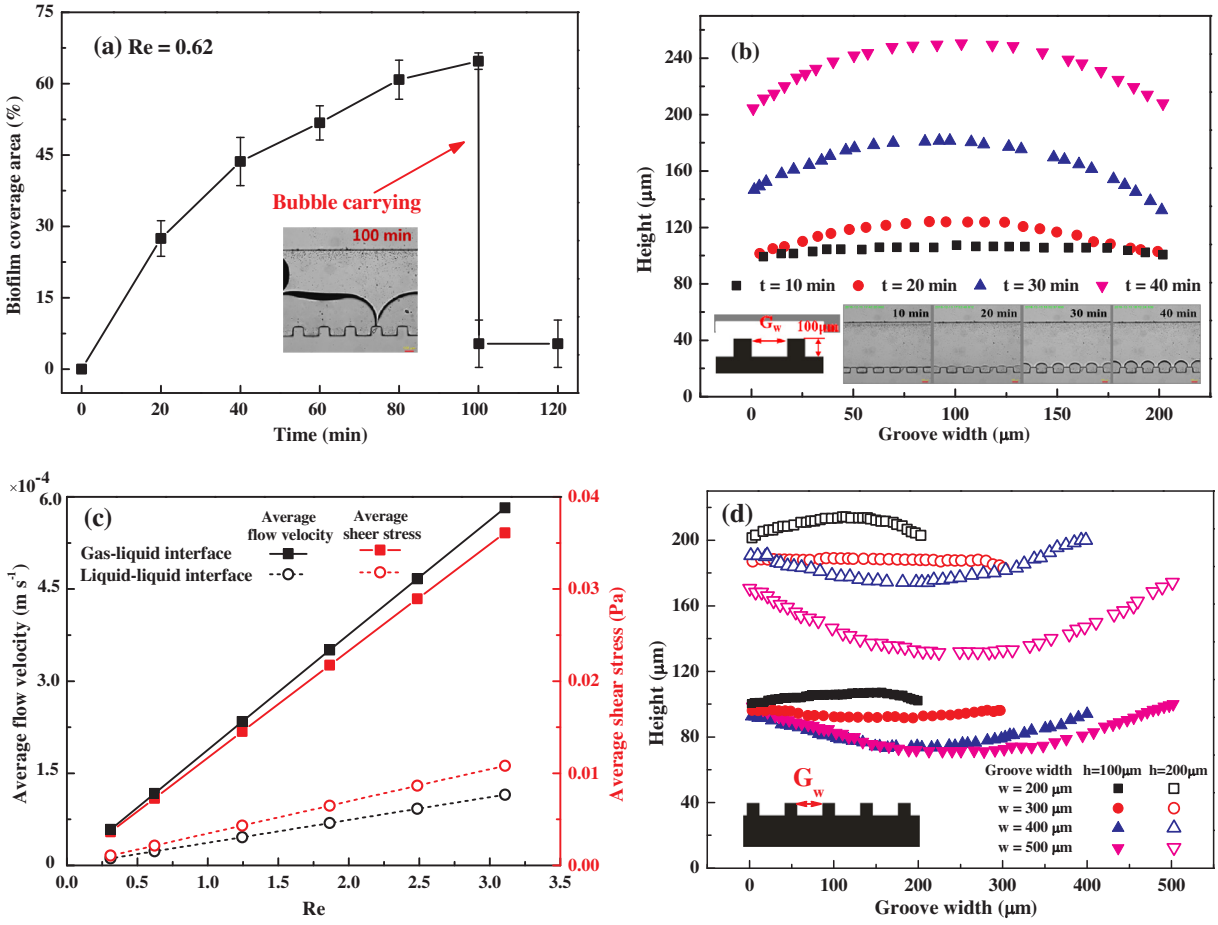


**Fig. 2.** The changes of microalgae initial attachment (a), gas-liquid interface (b) and the average flow rate and average shear stress of gas-liquid interface and liquid phase (c) on the U-grooves (h = 100 μm, w = 200 μm), and the effects of U-grooves sizes on the location of gas-liquid interface (d).

was chosen based on the Navier–Stokes and continuity equations assuming Newtonian incompressible fluid for this case. The boundary conditions were inlet velocity boundary, outlet pressure boundary (1 atm) and no slip wall boundaries (u = 0).

## 3. Results and discussion

### 3.1. The initial dynamic attachment of microalgae cells on the substrate surfaces with U-grooves

The initial attachment of microalgae cells was first investigated on the U-grooves substrates in B-MPBRs via visualization experiments. It could be obtained from Fig. 2a that the attached microalgae cells on U-grooves substrate were increased over time. But a big bubble was observed in the MPBR after running 100 min, and almost all of the attached cells were carried off from the substrate surfaces by the gas-liquid interface of this fast-moving bubble. This phenomenon was named 'bubble carrying' (Zhao et al., 2015). In order to explore the reasons for this phenomenon, S-MPBRs were applied to easily observe the changes of gas-liquid interface during the initial attachment period. Due to the entrapped gas in the microgrooves and gas pressure was greater than liquid pressure on the gas-liquid interface (Bormashenko et al., 2007), microalgae suspension was not able to flow into the microgrooves. It could be observed in the insets of Fig. 2b that liquid pinned between the grooves gaps so that gas-liquid interfaces existed around the top edge of the grooves and changed over time. Then, the gas-liquid interface gradually enlarged and expanded outward, then coalesced into big bubbles. These bubbles rapidly swept through the MPBRs driven by the flowing microalgae suspension. This changing process of gas-liquid interface was similar with the results of Wang et al. (2014), the gas resided in the grooves was constantly out from the surfaces under the action of coming flow. In addition, it was found that since the liquid could not flow inside the grooves, microalgae cells were attached on the gas-liquid interfaces and moved with the interface location changes, so that the attached cells were swept off when the coalescent bubble run through the MPBR. On the other hand, the average flow velocity and shear stress of the grooves top edges were calculated (Fig. 2c) under some assumptions. The solid lines were the average flow velocity and shear stress of gap-liquid interface assuming that the interfaces were without displacement. The dotted lines were the average flow velocity and shear stress of liquid phase assuming that liquid could flow into the grooves. From the results of hydrodynamic numerical calculation, when the gas-liquid interface existed between top edges of grooves, the average shear stress was significantly greater than that of liquid phase. That is, microalgae cells could attach on the substrate surfaces with U-grooves only if the cells overcome the great resistance. Obviously, it was not beneficial for biofilm formation (Graba et al., 2013).

Subsequently, U-grooves substrates with different sizes were used to test the microalgae attachment (Fig. 2d). The groove depths were design as 100 μm and 200 μm for that the biofilm thickness were generally 100–200 μm. If the groove depth was too small, it would be similar to the flat substrate and would not act well as the "anchor" for microalgae attachment. And the groove widths were widen from 200 μm to 500 μm based the previous experiments in order to avoid the liquid pinning. From Fig. 2d, liquid pinned between the groove gaps all the same. Therefore, it can be concluded that U-grooves substrate was not suitable for microalgae biofilm formation and growth. On the other hand, the

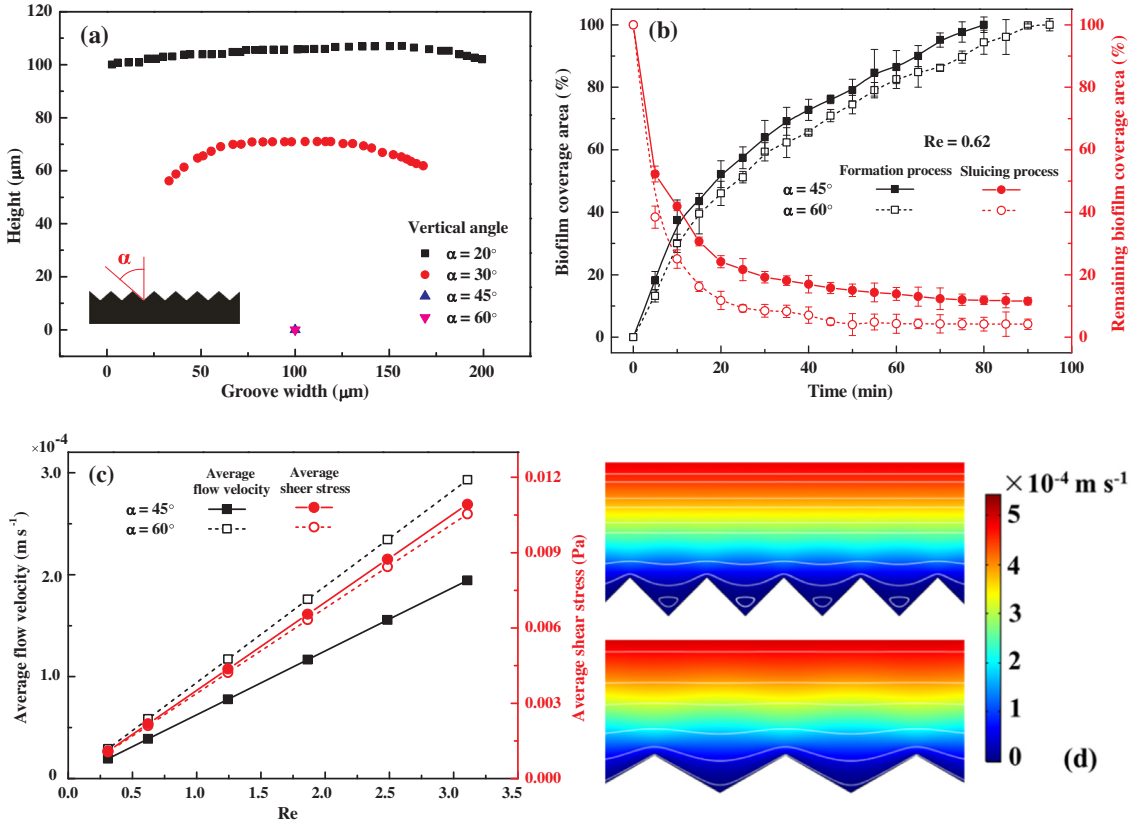


**Fig. 3.** The effects of the vertical angles of the V-grooves substrates on the locations of gas-liquid interface (a), the initial attachment of microalgae cells and biofilm attachment strength (b), the average flow rate and average shear stress (c) and the streamline distributions (d) on the substrate surfaces with V-grooves.

change of gas-liquid interface depended on the pressure difference between the gas phase and the liquid phase (Aljallis et al., 2013). Based on the Laplace-Young equation (Wang et al., 2014), this pressure difference was related to the apparent contact angle and vertical angle of grooves. Therefore, V-grooves was designed for the following experiments.

### *3.2. The initial dynamic attachment of microalgae cells on the substrate surfaces with V-grooves*

On account of the shortcomings of U-grooves substrates, the V-grooves substrates with different vertical angles were designed in this section. Fig. 3a is the location of gas-liquid interface on the V-grooves substrates with different vertical angles, after the microalgae suspension flowed into the B-MPBRs. The results showed the liquid levels tended to be lower with the increasing of V-groove vertical angles. The grooves could be totally filled with microalgae suspension when the V-grooves vertical angles were greater than 45°. The gas-liquid interface no longer existed around the substrate surfaces with grooves. Based on the conclusion of Section 3.1, once the gas-liquid interface absented around the substrate surfaces, bubble carrying wouldn't happen on the V-grooves substrate with the vertical angle of 45° and 60°. Therefore, these two kinds of V-grooves substrate were applied in the flowing experiments.

Fig. 3b showed the results of the initial attachment of microalgae cells and biofilm attachment strength in the S-MPBRs. The square symbols represented the changes of biofilm coverage area along with the microalgae suspension flowing with Re of 0.62. The circular symbols represented the changes of remaining biofilm coverage area under the water shear stress of 0.02 Pa. The results indicated that microalgae cells had a faster attachment rate on the 45° V-grooves substrate than that on the 60° V-grooves substrate. Microalgae biofilm coverage reached to 100% at the 80th min on the 45° V-grooves substrate, which was earlier than 100th min on 60° V-grooves substrate. As for the attachment strength, the more remaining biofilm coverage, the higher attachment strength the biofilm attached on the substrate. From the Fig. 3b, the remaining biofilm coverage on 45° V-grooves substrate was always more than that on 60° V-grooves substrate. After the action of water shear stress of 0.02 Pa for 90 min, the remaining biofilm coverage areas were 11.55% and 4.19% on the 45° and 60° V-grooves substrate respectively. Thus, microalgae biofilm had a higher attachment strength on the 45° V-grooved substrate than that on 60° V-grooves substrate.

The average flow rate (square symbols) and average shear stress (circular symbols) on the substrate surfaces with V-grooves were showed in Fig. 3c. As the trend shown in the Fig. 3c, the differences of the average shear stresses on these two kinds of substrates were quite small. Compared with the average shear stresses on U-grooves substrate surfaces, the average shear stresses on the substrate surfaces with V-grooves were very small. The hydraulic shear stress acted on the Biofilm on the V-grooves substrate (0.00105–0.01092 Pa) was lower than that on the U-lower (0.00108–0.03609 Pa). And the lower shear stress leaded to a faster attachment rate of microalgae cells (Wang et al., 2017). Therefore, V-grooves substrates were more suitable for biofilm formation and growth. However, the flow rates were lower on the substrate surfaces with 45° V-grooves, which indicated that the flow resistance on the substrate surfaces with 45° V-grooves were bigger than that on the substrate surfaces with 60° V-grooves. And the bigger resistance could well retain the microalgae cells in the flowing microalgae suspension, so that it was beneficial to microalgae attachment and biofilm formation. Furthermore, from the streamline distributions shown in Fig. 3d, vortex was observed inside the 45° V-grooves, which was absent inside the 60° V-grooves. Due to the existence of vortex, there were a series of 'dead zones' inside the grooves. Based on the

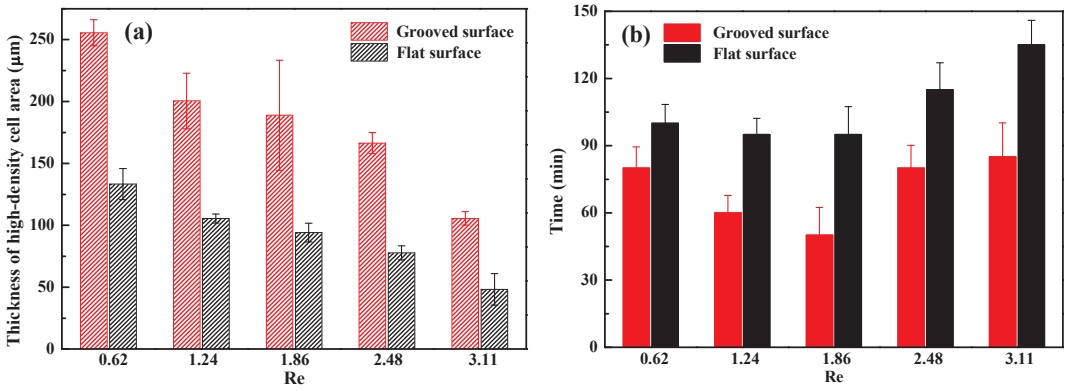


**Fig. 4.** The thickness of high-density cell area (a) and film-form time (b) on 45° V-grooves and flat substrates.

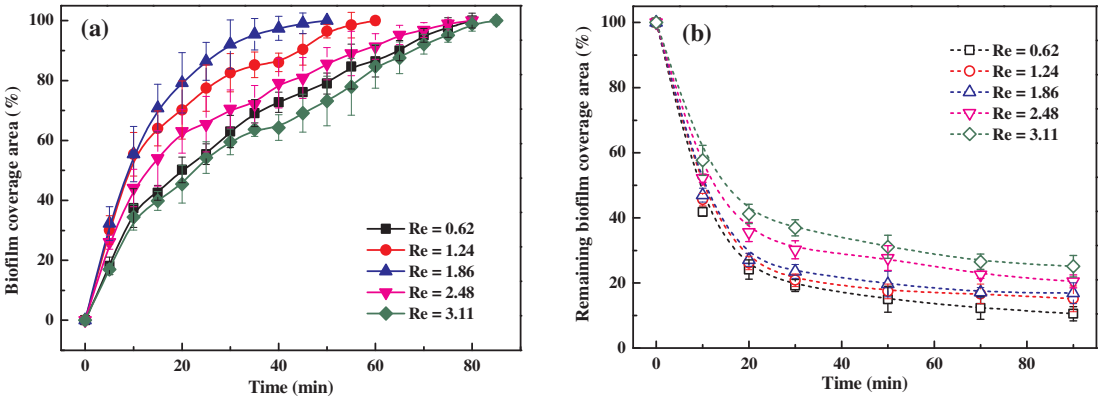


**Fig. 5.** Comparison of microalgae attachment rate under different Re (a) and attachment strength of the biofilms forming under different Re with a certain amount of shear stress, 0.02 Pa (b) on 45° V-grooves substrate.

results of Hadiyanto et al. (2013), the 'dead zones' could protect microalgae cells from carrying away by fluid. Therefore, the provoke not only promoted the cells attracted tightly and enhanced the biofilm attachment strength, but also ensured a higher transmission rate of nutrient and carbon between medium and cells inside the microgrooves for the dynamic flow. As for the streamline distributions on the substrate surfaces with 60° V-grooves, medium liquid directly flowed into the grooves, then outflowed from the grooves. Thus, the microalgae cells in the grooves were easily carried away and detached from the substrate surfaces, which were harmful to the biofilm formation and growth. Therefore, 45° V-grooves substrate was the optimizing substrate for microalgae biofilm cultivation due to the higher attachment rate and strength of microalgae cells on it.

### *3.3. The effects of medium flow on the initial attachment of microalgae on V-grooves substrate surfaces*

The V-grooves substrates chosen in last section were applied in this section. The visualization experiments were conducted to investigate the effects of flow rate on the initial attachment of microalgae on 45° V-grooves surfaces in the B-MPBRs (Fig. 4a) and S-MPBRs (Fig. 4b) respectively. Fig. 4a showed the comparison of thickness of high-density area on the 45° V-grooves and flat surfaces. The thickness of high-density area decreased as the Re increased both on the grooves and flat substrates. On the grooves substrates, the thickness of high-density area was 255.56 μm (Re = 0.62), 200.51 μm (Re = 1.24), 188.89 μm (Re = 1.86), 166.51 μm (Re = 2.48) and 105.55 μm (Re = 3.11), respectively. In addition, it was 133.33 μm (Re = 0.62), 105.56 μm (Re = 1.24), 94.05 μm (Re = 1.86), 77.75 μm (Re = 2.48) and 48.27 μm (Re = 3.11) on the flat substrates, respectively. These results indicated that the thickness of high-density area was inversely associated with Re both on grooves and flat substrates. Obviously, the thicknesses of high-density area on the grooves substrates were much thicker than that on the flat substrates at every Re in this study. For one thing, due to the increment of flow velocity, hydraulic shear stress tended higher around the wall surfaces and more microalgae cells were carried away by the liquid. For another, the increasing flow velocity led to the increment of the pressure gradient between mainstream and wall surfaces, according to the results by Wäsche et al. (2002), biofilm thickness became thinner and density under the action of rapid hydrodynamic condition. Thus, it resulted in the enhancement of the cell density in this region and the decrease of the high-density area. Fig. 4b showed the times when biofilm coverage area reached to 100% on the 45° V-grooves and flat surfaces in S-MPBRs. It took 80 min (Re = 0.62), 60 min (Re = 1.24), 50 min (Re = 1.86), 80 min (Re = 2.48) and 85 min (Re = 3.11) on the grooves substrates. Meanwhile, it took 100 min (Re = 0.62), 95 min (Re = 1.24), 95 min (Re = 1.86), 115 min (Re = 2.48) and 135 min (Re = 3.11) on the flat substrates. The form-film times on V-grooves substrates were all shorter than that on the flat substrates. Therefore, these results confirmed that V-grooves substrates possesses distinct advantages for biofilm attachment compared with flat substrates.

More concretely, Fig. 5a described the changes of biofilm coverage area over time under different Re in S-MPBRs. The results suggested that the Re had a significant impact on microalgae cell attachment and biofilm formation. As Re increased from 0.62 to 1.86, the film-form time gradually decreased from 80 min to 50 min. The attachment rates of microalgae cells were decreased with the increment of Re. However, the film-form time might be extended if the Re is excessive. As the Re further increased to 3.11, the film-form time increased to 85 min. And the attachment rates of microalgae cells were increased with the increment of Re. This may attributed that shear stress and flow velocity

were small under the low Re, which had few effects on microalgae attachment. Moreover, with the flow rate increasing, more microalgae cells passed through the substrate surfaces. Hence, the probability of collision between microalgae and substrates went up leading to the increment of microalgae attachment rate. However, excessive flow rate would enhance the hydraulic shear stress, which was detrimental to the microalgae attachment. That delayed the time when biofilm coverage reached to 100%. After the substrate surfaces were 100% covered by microalgae cells under different Re, the sterile water was pumped into the MPBRs with the shear stress of 0.02 Pa to investigate the biofilm attachment strength. As shown in Fig. 5b, the remaining biofilm coverage areas were 10.55%, 15.15%, 16.87%, 20.48% and 25.14% under the Re of 0.62, 1.24, 1.86, 2.48 and 3.11 after 90 min washing. Obviously, the attachment strength of microalgae biofilm forming under higher Re was stronger, so that they were able to resist higher hydraulic shear stress. That was likely attributed that as a stress factor, shear stress could promote extracellular polymeric substances (EPS) secretion, then EPS surround the biofilm and result in denser biofilm microstructure which made cells adhered each other more compactly and biofilm attach more tightly on the substrate surfaces (Kesaano and Sims, 2014). Therefore, on account of biofilm attachment strength, dynamic film-form method was better than the static sedimentation for biofilm formation.

### 3.4. The effects of inlet flow rate on microalgae biofilm growth on V-grooves surfaces in biofilm cultivation system

In this section, the experiments, the microalgae biofilm growth on the flat and groove substrates were conducted respectively under three Re (0.62, 1.86, 3.11). Fig. 6 showed the biofilm biomass concentration on the 45° V-grooves substrates (solid lines) and flat substrates (dotted lines). After 18 days cultivation, biofilm biomass concentrations were 139.46 g $m^{-2}$ and 134.51 g $m^{-2}$ on grooves and flat substrates respectively under the Re of 0.62 (Fig. 6a). Biofilm biomass concentrations were 154.45 g $m^{-2}$ and 143.37 g $m^{-2}$ on grooves and flat substrates respectively under the Re of 1.86 (Fig. 6b). Biofilm biomass concentrations were 165.84 g $m^{-2}$ and 145.11 g $m^{-2}$ on grooves and flat substrates respectively under the Re of 3.11 (Fig. 6c). And the biomass concentration was increased by 14.29%. It was observed the biofilm biomass concentration on grooves substrates were all higher than that on flat substrates. The increasing gap between the biofilm biomass concentration on grooves and flat was more apparent with the increment of Re. This was because that hydraulic shear stresses were increased with the Re increasing, so that the bigger the shear stress, the significant impact it had on the biofilm growth. The attachment strength of the biofilm on the grooves substrates was better than that on the flat substrate, so that biofilm still grown well under the higher Re. Conversely, biofilm on the flat substrate couldn't grow well as that on the grooves substrate. As shown in Fig. 6c, biofilm on the flat surface grown slowly during the early growth phase due to the large shear stress. Along with the biofilm growth, EPS was produced and bounded the microalgae cells together. It was conducted to enhance the biofilm attachment strength and the stress resistance (You et al., 2015). Thus, the differences of biofilm biomass concentrations on grooves and flat substrates were decreased during the later growth phase. In summary, with the increment of shear stress, the advantages of grooves substrate became more and more significant. On the other hand, biofilm biomass concentrations were increased with the increment of Re both on grooves substrates and flat substrates. That was due to the reasons that medium flow carried away the oxygen and other waste metabolites released by microalgae cells growth and avoided the accumulation of metabolic products, which minimized the possibility of product inhibition of the reactions (Zheng et al., 2016). Additionally, dynamic flow was able to refresh the cultivation medium and improve the nutrients concentration. Thus, appropriate flow rate had positive impacts on microalgae biofilm formation and growth.

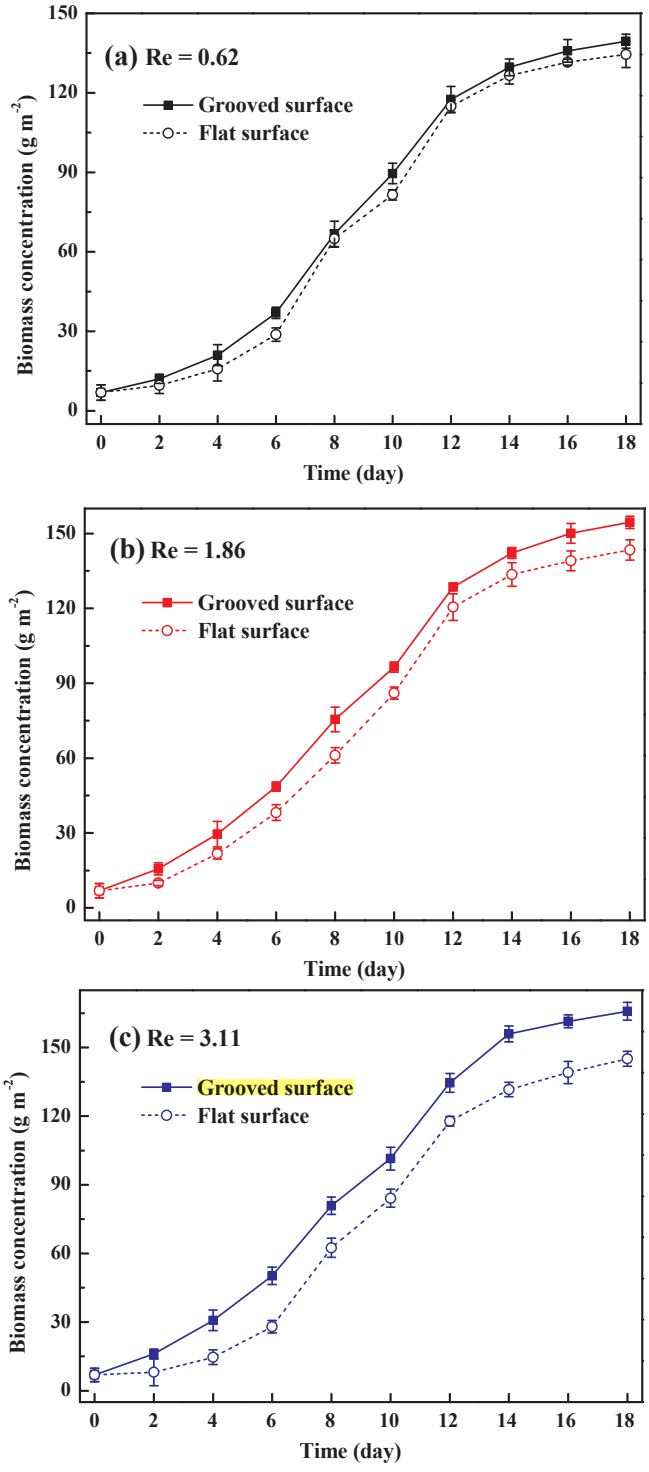


**Fig. 6.** Cooperation of biofilm biomass concentration on grooves and flat substrates under the Re of 0.62 (a), 1.86 (b), 3.11 (c).

Furthermore, the results of microalgae biofilm biomass productivity in this study were compared with that in the previous researches. Zheng et al. (2017) and Schnurr et al. (2016) chose flat glass and plastic surfaces as microalgae attaching substrate. The biomass concentration could achieve 22.42 g $m^{-2}$ and 52 g $m^{-2}$, respectively. Lan et al. (2017) proposed a microalgae biofilm cultivation approach on rough shifting sand surface, resulting in a biomass concentration of 11 g $m^{-2}$ and the biomass production of 0.4 g $m^{-2}$ $day^{-1}$. Gross et al. (2016) investigated microalgae biofilm growth on several meshy materials. The results

showed the biomass concentration was 28–10 g $m^{-2}$ and the biomass production was 4.0–4.3 g $m^{-2}$ $day^{-1}$ on the substrate of nylon with the mesh of 0.5 mm. Wang et al. (2015) cultivated microalgae biofilm on the porous filter paper. The biomass concentration and production reached to 107.6 g $m^{-2}$ and 8.8 g $m^{-2}$ $day^{-1}$. However, in this study, by inducing microgrooves into surface, the biomass concentration could up to 165.84 g $m^{-2}$. Obviously, substrate surface with microgrooves proposed in this study was a better choose for microalgae biofilm cultivation.

## 4. Conclusions

The substrates with V-grooves enhanced the biofilm attachment strength for the fact that the microgrooves acted as anchor points and created vortex for microalgae cells sheltered from shear stresses, which were beneficial to biofilm formation and growth. Compared with that on the flat surface, the initial attachment time was shortened from 135 min to 50 min on the substrates with 45° V-grooves. And the biomass concentration increased by 14.29% to 165.84 g $m^{-2}$ compared with that on flat substrate with the inlet flow rate of 5 ml $min^{-1}$. This work could quantitatively guide for substrate choice for microalgae biofilm cultivation.

## Acknowledgements

The authors gratefully acknowledge the financial support from the Project of the International Cooperation and Exchanges NSFC, China (No. 51561145013), and the National Science Foundation for Young Scientists of China, China (No. 51606020).

## References

Ahsan, S.S., Pereyra, B., Jung, E.E., Erickson, D., 2014. Engineered surface scatterers in edge-lit slab waveguides to improve light delivery in algae cultivation. Opt. Express 22 (106), A1526–A1537.
Aljallis, E., Sarshar, M.A., Datla, R., Sikka, V., Jones, A., Choi, C.H., 2013. Experimental study of skin friction drag reduction on superhydrophobic flat plates in high Reynolds number boundary layer flow. Phys. Fluids 25 (2), 025103.
Bing, T., Yu, C., Bin, L., Zhao, Y., Feng, X., Huang, S., Fu, F., Ding, J., Chen, C., Ping, L., 2016. Essential factors of an integrated moving bed biofilm reactor–membrane bioreactor: adhesion characteristics and microbial community of the biofilm. Bioresour. Technol. 211, 574–583.
Bormashenko, E., Pogreb, R., Whyman, G., Bormashenko, Y., Erlich, M., 2007. Vibration-induced Cassie-Wenzel wetting transition on rough surfaces. Appl. Phys. Lett. 90 (20), 201917.
Cao, J., Yuan, W., Pei, Z.J., Davis, T., Cui, Y., Beltran, M., 2009. A preliminary study of the effect of surface texture on algae cell attachment for a mechanical-biological energy manufacturing system. J. Manuf. Sci. Eng. 131 (6), 2461–2464.
Carl, C., Poole, A.J., Sexton, B.A., Glenn, F.L., Vucko, M.J., Williams, M.R., Whalan, S., Nys, R.D., 2012. Enhancing the settlement and attachment strength of pediveligers of *Mytilus galloprovincialis* bychanging surface wettability and microtopography. Biofouling 28 (2), 175–186.
Chen, H., Fu, Q., Liao, Q., Zhang, H., Huang, Y., Xia, A., Zhu, X., 2017. Rheological properties of microalgae slurry for application in hydrothermal pretreatment systems. Bioresour. Technol. 249, 599–604.
Crawford, R.J., Webb, H.K., Truong, V.K., Hasan, J., Ivanova, E.P., 2012. Surface topographical factors influencing bacterial attachment. Adv. Colloid Interface 179–182 (13), 142–149.
Eun, Y.J., Weibel, D.B., 2009. Fabrication of microbial biofilm arrays by geometric control of cell adhesion. Langmuir 25 (8), 4643.
Gao, F., Yang, Z.H., Li, C., Zeng, G.M., Ma, D.H., Zhou, L., 2015. A novel algal biofilm membrane photobioreactor for attached microalgae growth and nutrients removal from secondary effluent. Bioresour. Technol. 179, 8–12.
Graba, M., Sauvage, S., Moulin, F.Y., Urrea, G., Sabater, S., Sanchez-Pérez, J.M., 2013. Interaction between local hydrodynamics and algal community in epilithic biofilm. Water Res. 47 (7), 2153–2163.
Gross, M., Zhao, X., Mascarenhas, V., Wen, Z.Y., 2016. Effects of the surface physicochemical properties and the surface textures on the initial colonization and the attached growth in algal biofilm. Biotechnol. Biofuels 9 (1), 38.
Gross, M., Jarboe, D., Wen, Z., 2015. Biofilm-based algal cultivation systems. Appl. Microbiol. Biotechnol. 99 (14), 5781–5789.
Hadiyanto, H., Elmore, S., Van Gerven, T., Stankiewicz, A., 2013. Hydrodynamic evaluations in high rate algae pond (HRAP) design. Chem. Eng. J. 217, 231–239.
Hou, S., Gu, H., Smith, C., Ren, D., 2011. Microtopographic patterns affect *Escherichia coli* biofilm formation on poly(dimethylsiloxane) surfaces. Langmuir 27 (6), 2686–2691.
Kardel, K., 2016. An analytical and experimental study on 3D-printed custom surfaces for benthic algal biofilms (Diss).
Kesaano, M., Sims, R.C., 2014. Algal biofilm based technology for wastewater treatment. Algal Res. 5 (1), 231–240.
Kim, J., Park, H.D., Chung, S., 2012. Microfluidic approaches to bacterial biofilm formation. Molecules 17 (8), 9818–9834.
Lan, S., Li, W., Yang, H., Zhang, D., Hu, C., 2017. A new biofilm based microalgal cultivation approach on shifting sand surface for desert cyanobacterium microcoleus vaginatus. Bioresour. Technol. 238, 602.
Liao, Q., Chang, H.X., Fu, Q., Huang, Y., Xia, A., Zhu, X., Zhong, N., 2018. Physiological-phased kinetic characteristics of microalgae Chlorella vulgaris growth and lipid synthesis considering synergistic effects of light, carbon and nutrients. Bioresour. Technol. 250, 583–590.
Ngene, I.S., Lammertink, R.G.H., Wessling, M., Meer, W.G.J.V.D., 2010. Particle deposition and biofilm formation on microstructured membranes. J. Membr. Sci. 364 (1–2), 43–51.
Park, A., Jeong, H.H., Lee, J., Kim, K.P., Lee, C.S., 2011. Effect of shear stress on the formation of bacterial biofilm in a microfluidic channel. Biochip J. 5 (3), 236–241.
Sathananthan, S., Genin, S.N., Aitchison, J.S., Allen, D.G., 2013. Micro-structured surfaces for algal biofilm growth. SPIE Micro + Nano Materials, Devices, and Applications. Int. Soc. Opt. Photonics. pp. 892350–892350-9.
Schnurr, P.J., Molenda, O., Edwards, E., Espie, G.S., Allen, D.G., 2016. Improved biomass productivity in algal biofilms through synergistic interactions between photon flux density and carbon dioxide concentration. Bioresour. Technol. 219, 72.
Schnurr, P.J., Allen, D.G., 2015. Factors affecting algae biofilm growth and lipid production: a review. Renewable Sustainable Energy Rev. 52, 418–429.
Shayan, S.I., Agblevor, F.A., Bertin, L., Sims, R.C., 2016. Hydraulic retention time effects on wastewater nutrient removal and bioproduct production via rotating algal biofilm reactor. Bioresour. Technol. 211, 527–533.
Shen, Y., Xu, X., Zhao, Y., Lin, X., 2013. Influence of algae species, substrata and culture conditions on attached microalgal culture. Bioproc. Biosyst. Eng. 37 (3), 441–450.
Sun, Y., Huang, Y., Liao, Q., Xia, A., Fu, Q., Zhu, X., Fu, J., 2018. Boosting Nannochloropsis oculata growth and lipid accumulation in a lab-scale open raceway pond characterized by improved light distributions employing built-in planar waveguide modules. Bioresour. Technol. 249, 880–889.
Wang, B., Wang, J.D., Chen, D.R., 2014. Drag reduction on hydrophobic transverse grooved surface by underwater gas formed naturally. Acta Phys. Sin. 63 74702 074702.
Wang, J., Liu, W., Liu, T., 2017. Biofilm based attached cultivation technology for microalgal biorefineries–A review. Bioresour. Technol. 244, 1245–1253.
Wang, J.F., Liu, J.L., Liu, T.Z., 2015. The difference in effective light penetration may explain the superiority in photosynthetic efficiency of attached cultivation over the conventional open pond for microalgae. Biotechnol. Biofuels 8 (1), 49.
Wäsche, S., Horn, H., Hempel, D.C., 2002. Influence of growth conditions on biofilm development and mass transfer at the bulk/biofilm interface. Water Res. 36 (19), 4775–4784.
You, G., Hou, J., Xu, Y., Wang, C., Wang, P., Miao, L., Ao, Y., Li, Y., Lv, B., 2015. Effects of $CeO_2$ nanoparticles on production and physicochemical characteristics of extracellular polymeric substances in biofilms in sequencing batch biofilm reactor. Bioresour. Technol. 194, 91–98.
Zhang, C., Zhu, X., Liao, Q., Wang, Y., Li, J., Ding, Y., Wang, H., 2010. Performance of a groove-type photobioreactor for hydrogen production by immobilized photosynthetic bacteria. Int. J. Hydrogen Energy 35 (11), 5284–5292.
Zhao, S., Ding, Y.D., Chen, R., Liao, Q., Zhu, X., 2015. Dynamic behaviors of $CO_2$ bubbles coalescing at two parallel capillary orifices in microalgae suspension. Int. J. Heat Mass Transf. 90, 1001–1008.
Zheng, Y., Huang, Y., Liao, Q., Fu, Q., Xia, A., Zhu, X., 2017. Impact of the accumulation and adhesion of released oxygen during *Scenedesmus obliquus* photosynthesis on biofilm formation and growth. Bioresour. Technol. 244, 198–205.
Zheng, Y., Huang, Y., Liao, Q., Zhu, X., Fu, Q., Xia, A., 2016. Effects of wettability on the growth of *Scenedesmus obliquus* biofilm attached on glass surface coated with polytetrafluoroethylene emulsion. Int. J. Hydrogen Energy 41 (46), 21728–21735.